International Journal Evolving Sustainable and Renewable Energy Solutions

PRIME OPEN ACCESS

Volume 1, Issue 2

Research Article

Date of Submission: 10 June, 2025
Date of Acceptance: 30 June, 2025
Date of Publication: 11 July, 2025

Resonant Tunneling Frequency and Current in a Nanostructured Diode with a Two-Fold Right Triangular Barrier

A. M. Elabsy* and M. T. Attia

Department of Physics, Mansoura University, Egypt

***Corresponding Author:**
A. M. Elabsy, Department of Physics, Mansoura University, Egypt.

Citation: Elabsy, A., M., Attia, M., T. (2025). Resonant Tunneling Frequency and Current in a Nanostructured Diode with a Two-Fold Right Triangular Barrier. *Int J Evol Sus Renew Energy Sol, 1*(2), 01-11.

Abstract
The resonant tunneling frequency and electric current were studied in a nanostructured diode containing a two-fold symmetrical right triangular barrier made of AlyGa1-yAs/GaAs/AlyGa1-yAs semiconductors. The complex energy method was employed to determine the quasi-energy states, utilizing varying effective masses. The resonant tunneling energy decreased exponentially with increasing well width when the barrier thickness was fixed. Keeping the well width and barrier thickness constant and increasing the aluminum concentration, decreases the resonant tunneling frequency while increasing the resonant tunneling energy. The resonant tunneling frequency was increased to a higher terahertz range by reducing the barrier thickness and well width. Wider wells and thicker barriers result in lower resonant frequencies. The resonant tunneling current was analyzed and found to be significantly influenced by the diode parameters, including aluminum content, well width, and barrier thickness in the collector region. The resonant tunneling current behavior aligned well with previous literature findings. It is noted that the structural features of the nanostructured diode, which has a two-fold symmetrical right triangular barrier, can be adjusted to function within the targeted frequency range and the peak tunneling current.

Keywords: Resonant Tunneling Diode, Resonant Frequency, Resonant Tunneling Current, Nanostructure Materials

Introduction
Conventional diodes (CDs) are devices that contain two regions, namely anode and cathode, and can conduct current in the forward direction instead of the reverse direction. However, CDs are not suitable for ultrafast applications because of their low signal gain. A resonant tunneling diode (RTD) employs the resonant tunneling property. Resonant tunneling occurs at certain resonant energy levels, corresponding to the doping level and the width of the quantum well and is mainly characterized by the negative differential resistance in the I-V characteristics. A high peak current to valley current ratio (Ip/Iv) is desirable because a high value indicates a large RTD gain and a significant negative differential resistance and also implies a small valley current, which means less leakage current and reduced power loss [1]. The advantages of RTDs over both CDs and triodes are their low power, high speed, and reduced dimensions that avoid the problems of heat and parasitic effects. RTDs can reach frequencies in the THz range above that associated with transistors that usually operate in the GHz range, which allows them to be part of a variety of nanotechnology applications such as high-speed communication systems, high-resolution radars, and low-level imaging systems [2, 3]. In addition, RTDs have significant advantages over CDs when high reverse voltages are applied; there is a very high leakage current in CDs, while for RTDs, there is a symmetric I-V response when forward as well as a reverse bias voltage is applied. Therefore, the leakage current is minimized, and RTDs are considered excellent rectifiers. For high-frequency operation, very high peak current densities are obtained by reducing the QW thickness and increasing the emitter doping level [2,4]. Resonant tunneling in heterostructure semiconductor materials has received a lot of attention

after the proposal of periodic potentials depending on the change in material type or doping type [5]. The periodicity of potentials and the development of deposition techniques yield heterostructure superlattices [6,7]. Many researchers have reported experimental evidence of the phenomenon of resonant tunneling of electrons and holes in quantum wells bounded by potential barriers, which appear as negative resistance regions in the current-voltage characteristics [8-11]. Computational and theoretical analysis have also been addressed to study the resonant tunneling phenomena in heterostructures [12-19]. With the novel development of growth techniques, researchers are now able to investigate the resonant tunneling in profile-based nanomaterials such as quantum wells, quantum wires, quantum dots, carbon nanotubes (CNTs), and double-barrier triangular semiconductor heterostructures [20-34]. Recently, Elabsy and Attia have reported resonant tunneling in a double-barrier triangular nanostructure in a free electric field and in the presence of an electric field [35,36]. The resonant tunneling effect has also been reported in graphene superlattice heterostructures and in transition metal dichalcogenides (TDMs) [37,38]. Terahertz frequency devices have many applications in today's life, such as wireless communications, imaging systems, radar systems, and chemical and biotechnology [39-41]. Therefore, the present study aims to go beyond the previous work and proposes a nanostructured diode with a two-fold symmetrical right triangular barrier to investigate the resonant tunneling frequency, the associated resonant energy, and the resonant tunneling current of electrons through it [32-36].

Theory

It is known that temperature, pressure, and applied bias are important parameters that influence the performance of nanostructure diodes, but in this work, we are looking for efficiency, not precision. Therefore, the present analysis considers constant temperature, pressure, and zero electric field. The units used are the atomic units, in which the unit of energy is Hartree, and the unit of length is Bohr radius, with e (electronic charge) = m0 (mass of a free electron) = $\hbar$ (reduced Plank's constant) = 1, unless stated. The present study employs the effective mass theory with the correct masses of the electron in each region of the present diode structure and applies the complex energy technique to compute the required energies and their associated frequencies [18,35,36]. The energy band gap profile for the two-fold symmetrical right triangular barrier diode composed of $Al_yGa_{1-y}As/GaAs/Al_yGa_{1-y}As$ semiconductor heterostructure with z-axis is taken as the direction of growth and the potential barrier height, U0, well thickness, 2a, and barrier thickness, b, as sketched in Figure 1.

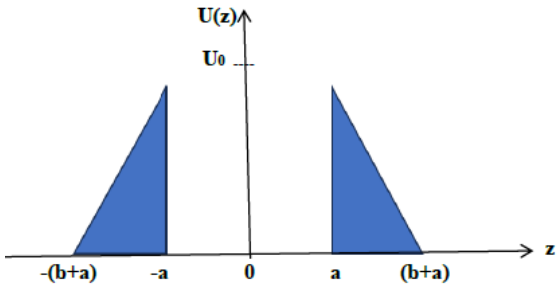

Figure 1: Symmetric Two-Fold Right-Triangular Barrier Nanostructured Diode with a Barrier Height of u_0, a Well Width of 2a, and a Barrier Thickness of b, with the Z-Axis Being the Growth Direction

The total symmetric potential energy, U(z) has the form

$$U(z) = \begin{cases} 0; & 0 \le |z| \le a \\ \frac{U_0}{b}(b + a - z); & a < |z| \le a + b \\ 0; & |z| > a + b \end{cases} \quad (1)$$

The general form of Schrödinger equation has the form [35], [36], and [42]

$$-\frac{1}{2}\frac{d}{dz}\frac{1}{m_p^*(z)}\frac{d\Phi_n(z)}{dz} + U(z)\,\Phi_n(z) = E_n\,\Phi_n(z) \quad (2)$$

Where the subscript, p refers to the well region, a, or barrier region, b, and $m_p^*(z)$ stands for the effective mass of the carriers (electrons) in the well p=a or the barrier p=b region, which has the form [43].

$$m_a^* = 0.067 \; and \; m_b^* = m_a^* + 0.083\,y, \quad (3)$$

since y is the aluminum mole fraction in the barrier $Al_yGa_{1-y}As$ region. The barrier height, U_0, depends on the aluminum content (concentration) in the barrier AlyGa1-yAs region, as given by Lee et al. [44]

$$U_0 = 0.658\,\Delta E_g^{\Gamma}(y), \quad (4)$$

Where $\Delta E_g^{\Gamma}(y)$ is the energy band gap discontinuity between the conduction energy bands of the GaAs and $Al_yGa_{1-y}As$ materials at the Γ-point and is determined from the relation [45]

$$\Delta E_g^{\Gamma}(y) = 1.155\, y + 0.37\, y^2. \tag{5}$$

$\Phi_n(x)$ is the position probability amplitude wavefunction and E_n is the corresponding allowed energy for the required energy n-state since the subscript (n = 1) stands for the lowest (ground) energy state and (n = 2) to the first excited state.

The wavefunction corresponding to the (emitter) well region, $0 \le |z| \le a$, has the even solution of Eq. (2) as

$$\Phi(x) = A_1 cos(q_1 z); \qquad 0 \le |z| \le a \tag{6}$$

Where A_1 is a constant and q_1 is the propagation wave number of electrons in the well region which has the form

$$q_1 = (2m_a^* E_n)^{1/2} \tag{7}$$

In the (collector) well region $|z| > a + b$, the solution of Eq. (2), takes the form

$$\Phi(z) = A_4\, e^{iq_1 z}; \qquad |z| > a + b \tag{8}$$

where A_4 is a constant to be determined.

In the barrier triangular regions, $a < |z| \le a + b$, Eq. (2) becomes

$$\frac{d^2\Phi_n(z)}{dz^2} + \frac{2m_b^* U_0}{b}[z + \Omega]\,\Phi_n(z) = 0, \tag{9}$$

Since,

$$\Omega = \frac{b}{U_0}E_n - (a + b), \tag{10}$$

Introduce the parameters,

$$\Lambda = \left(\frac{2m_b^* U_0}{b}\right)^{1/3}, \tag{11}$$

and

$$\chi = -\Lambda(z + \Omega), \tag{12}$$

Eq. (9) takes the form of Airy's equation as

$$\frac{d^2\Phi_n(\chi)}{d\chi^2} - \chi\,\Phi_n(\chi) = 0\,. \tag{13}$$

The general solution of equation (13) is

$$\Phi_n(\chi) = A_2\, Ai(\chi) + A_3\, Bi(\chi). \tag{14}$$

Where A_2 and A_3 are constants to be determined.

Then the total wavefunction, $\Phi(z)$ has the form

$$\Phi(z) = \begin{cases} A_1 cos(q_1 z); & 0 \le |z| \le a \\ A_2\, Ai(\chi) + A_3\, Bi(\chi); & a < |z| \le a + b \\ A_4\, e^{iq_1 z}; & |z| > a + b \end{cases} \tag{15}$$

Imposing the boundary conditions on the wavefunctions, $\Phi_n(z)$ at the triangle face z = a, one obtains

$$A_1 \cos\mu - A_2\, Ai(\lambda_1) - A_3\, Bi(\lambda_1) = 0 \tag{16}$$

Where

$$\mu = q_1 a\,, \tag{17}$$

and

$$\lambda_1 = -\Lambda(a + \Omega). \tag{18}$$

Applying the boundary conditions on the derivative of the wavefunctions, $\frac{1}{m_p^*(z)}\frac{d\Phi_n(z)}{dz}$ at the same triangle face z = a, or

$$\frac{1}{m_a^*}\frac{d}{dz}\,[A_1 cos(q_1 z)]|_a = \frac{1}{m_b^*}\frac{d}{dz}\,[A_2\, Ai(\chi) + A_3\, Bi(\chi)]|_a \tag{19}$$

which becomes

$$-\delta\, A_1 \sin\mu + A_2\, Ai'(\lambda_1) + A_3\, Bi'(\lambda_1) = 0 \tag{20}$$

where

$$\delta = q_1 \frac{\sigma}{\Lambda} \tag{21}$$

since

$$\sigma = m_b^*/m_a^* \tag{22}$$

is the effective mass ratio and Ai' is the derivative of Airy's function

Similarly, by imposing the boundary conditions on the wavefunctions, $\Phi_n(z)$ at the triangle edge z = a+b, one gets

$$A_2\, Ai(\lambda_2) + A_3\, Bi(\lambda_2) - A_4\, e^{i\nu} = 0. \tag{23}$$

Where

$$\nu = q_1\,\mu + b, \text{ and} \tag{24}$$

$$\lambda_2 = \lambda_1 - b\Lambda. \tag{25}$$

By imposing the boundary conditions on the derivative of the wavefunctions, $\frac{1}{m_p^*(z)}\frac{d\Phi_n(z)}{dz}$ at the same triangle edge z = a + b, or

$$\frac{1}{m_b^*}\frac{d}{dz}\,[A_2\, Ai(\chi) + A_3\, Bi(\chi)]|_{a+b} = \frac{1}{m_a^*}\frac{d}{dz}\,[A_4\, e^{iq_1 z}]\Big|_{a+b} \tag{26}$$

it becomes

$$A_2\, Ai'(\lambda_2) + A_3\, Bi'(\lambda_2) + (i\,\delta)\, A_4\, e^{i\nu} = 0 \tag{27}$$

Equations (16), (20), (23), and (27) form a matrix equation with non-vanishing coefficients, $A_1, A_2, A_3, and\ A_4$. The matrix equation has only a solution if the determinant of the coefficients vanishes as

$$\begin{vmatrix} \cos\mu & -Ai(\lambda_1) & -Bi(\lambda_1) & 0 \\ -\delta\,\sin\mu & Ai'(\lambda_1) & Bi'(\lambda_1) & 0 \\ 0 & Ai(\lambda_2) & Bi(\lambda_2) & -e^{i\nu} \\ 0 & Ai'(\lambda_2) & Bi'(\lambda_2) & (i\,\delta)e^{i\nu} \end{vmatrix} = 0 \tag{28}$$

Solving the determinant Eq. (28), one obtains a transcendental equation for the even resonant tunneling energies and their corresponding frequencies in the form

$$\tan(\mu) = \frac{T_1 \cdot B_i'(\lambda_1) - T_2 \cdot A_i'(\lambda_1)}{\delta[T_1 \cdot B_i(\lambda_1) - T_2 \cdot A_i(\lambda_1)]}. \quad (29)$$

Where

$$T_1 = i\delta A_i(\lambda_2) + A_i'(\lambda_2), \quad (30)$$

$$T_2 = i\delta B_i(\lambda_2) + B_i'(\lambda_2), \quad (31)$$

In the above equations A_i' and B_i' are the derivative of Airy's functions, Ai and Bi with respect to z, respectively.

For the odd solution, one replaces the wavefunction in the first-well (emitter) region ($0 \le |z| \le a$ by

$$\Phi(z) = D \sin(q_1 z). \quad (32)$$

Where D is an arbitrary constant to be determined.

Applying the boundary conditions on the wavefunctions, $\Phi_n(z)$ at the triangle face z = a, one gets

$$D \sin\mu - C_2\, Ai(\lambda_1) - C_3\, Bi(\lambda_1) = 0 \quad (33)$$

By imposing the boundary conditions on the derivative of the wavefunctions, $\frac{1}{m_p^*(z)} \frac{d\Phi_n(z)}{dz}$ at the triangle face z = a, yields

$$\delta\, D \cos\mu + C_2\, Ai'(\lambda_1) + C_3\, Bi'(\lambda_1) = 0 \quad (34)$$

Solving the set of equations, (33), (34), (23), and (27) one obtains the determinant for the odd solution as

$$\begin{vmatrix} \sin\mu & -Ai(\lambda_1) & -Bi(\lambda_1) & 0 \\ \delta\cos\mu & Ai'(\lambda_1) & Bi'(\lambda_1) & 0 \\ 0 & Ai(\lambda_2) & Bi(\lambda_2) & -e^{iv} \\ 0 & Ai'(\lambda_2) & Bi'(\lambda_2) & (i\,\delta)e^{iv} \end{vmatrix} \quad (35)$$

Following the same procedures by solving the determinant Eq. (35), one can obtain a transcendental equation for the odd energy states and their associated frequencies in the form

$$\cot(\mu) = -\frac{T_1 \cdot B_i'(\lambda_1) - T_2 \cdot A_i'(\lambda_1)}{\delta[T_1 \cdot B_i(\lambda_1) - T_2 \cdot A_i(\lambda_1)]}. \quad (36)$$

The resonant tunneling current, Ir (given in Ampere), through the nanostructured diode with a two-fold symmetrical right triangular barrier with a barrier height of U_0, a well width of 2a, and a collector barrier thickness of b, is determined using the equation [46]

$$I_r = I_0\, f \exp(-2\,\rho b)\ (A) \quad (37)$$

Where

$$I_0 = 1.602\ x\ 10^{-19}\ (A/Hz) \quad (38)$$

f is the resonant tunneling frequency of electrons in the emitter layer, given in Hertz (Hz), b is the collector barrier thickness, and ρ is the decay constant in the collector layer, which is evaluated as

$$\rho = \sqrt{2\, m_1^*} U_0 \quad (39)$$

Results and Discussions

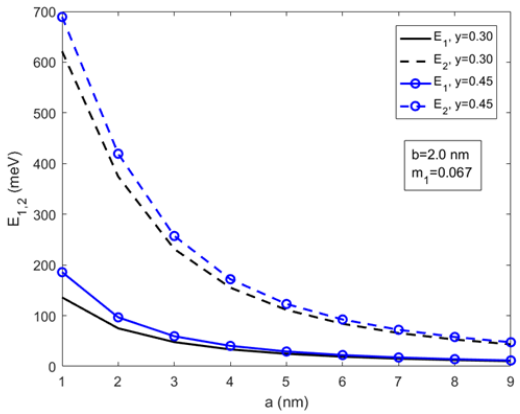

Figure 2: Variations of the Resonant Tunneling Energies of the Lowest State, E1(Mev) (Solid Lines), and the First Excited State, E2(Mev) (Dashed Lines), with the Well Half-Width, a in Nm for Two Aluminum Contents, Y=0.30 (Black Lines) and 0.45 (blue lines) at a Constant Barrier Thickness Of 2.0 Nm

Figure 2 shows the variation of the resonant tunneling energy of the lowest state, E1, and the first excited state, E2, in meV with the well half-width, a, in nm at a fixed barrier thickness, b = 2.0 nm for two aluminum contents (concentrations), y = 0.30 and 0.45. Both energy values decrease with increasing well half-width in an exponential decay trend. It is seen that increasing the aluminum content, y, enhances the barrier height, which increases the resonant tunneling energies of the two states (blue lines). It is also seen in Figure 2 that reducing the aluminum content in the diode barrier region, $Al^{y}Ga_{1-y}As$ decreases the barrier height, which in turn decreases the resonant tunneling energy for both the ground (lowest) state and the first excited state (black lines) in accordance with the concepts of quantum mechanics [47]. Additionally, one notes that the resonant tunneling energy of the first excited state (dashed line), regardless of the aluminum content, is larger than the energy associated with the lowest state (solid line).

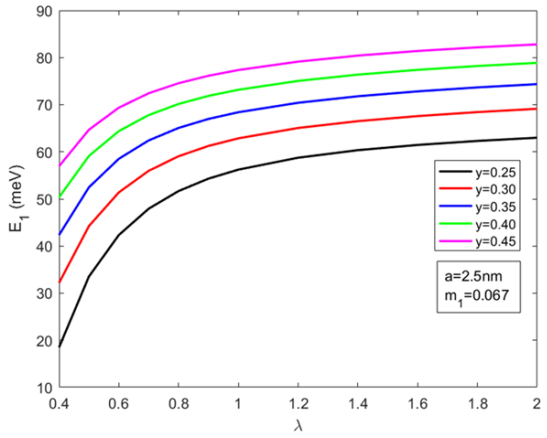

Figure 3: Dependence of the Lowest Resonant Tunneling Energy, E_1 (Mev) at a Constant Well Half-Width, a, of 2.5 Nm on t=the Ratio of the Barrier Thickness to the Well Half-Width, λ = b/a for Different Aluminum Contents, y = 0.25 (Black), 0.30 (Red), 0.35 (Blue), 0.40 (Green), And 0.45 (Purple)

Figure 3 presents the dependence of the lowest resonant tunneling energy, E_1 (meV), on the ratio of the barrier thickness to the well-half-width, λ = b/a, for different aluminum contents, y, at a constant well-half-width of 2.5 nm. It is shown in Figure 3 that increasing the ratio of the barrier thickness to the well half-width at a specific aluminum content results in an almost non-linear enhancement of the lowest resonant tunneling energy, E_1. It is also seen in Figure 3 that the lowest resonant energy, E_1, increases non-linearity with an increase in the ratio λ. The lowest energy, E1, increases almost linearly up to a specific value of the ratio of the barrier thickness to the well halfwidth (λ 0.6 nm), then slowly increases. Furthermore, for a fixed ratio λ, it is shown that increasing the aluminum content, y, enhances the lowest resonant tunneling energy, E_1. This is because increasing the aluminum content, y, leads to an enhancement of the barrier strength (height, U_0), which in turn increases the lowest resonant tunneling energy, E_1, in accordance with quantum mechanics concepts [47].

Figure 4 shows the variation of the resonant tunneling frequency of the lowest state, f_1, in THz, with the well half-width, a, in nm for different aluminum contents, y, with a constant barrier thickness of 2.0 nm. It can be seen in Figure 4 that at a fixed value of the aluminum content, y, in the barrier region of the right triangle diode, $Al_yGa_{1-y}As$, the frequency of the lowest resonant tunneling, f_1, decreases with increasing the well half-width, a. This finding is attributed to the enhancement

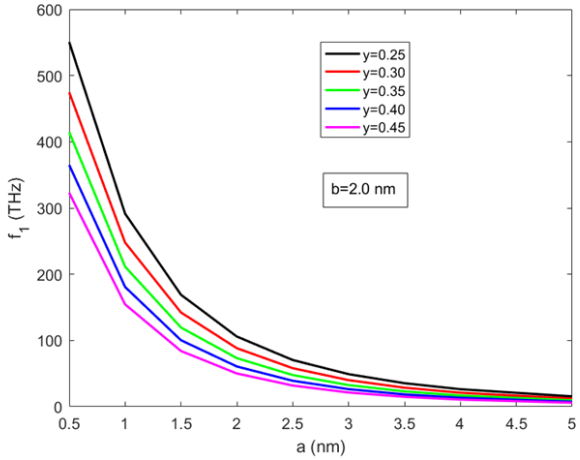

Figure 4: Variations of the Resonant Tunneling Frequency of the Lowest State, F_1 (thz) with the Well Half-Width a (Nm) at a Constant Barrier Thickness, B=2.0 Nm for Different Aluminum Contents, Y=0.25 (Black), 0.30 (Red), 0.35 (Green), 0.40 (Blue) and 0.45 (Purple)

of the resonant lifetime associated with the lowest state as the well half-width increases, leading to a decrease in the frequency, f_1. It is shown in Figure 4 that for fixed values of the well-half width and the barrier thickness, increasing the aluminum content leads to a decrease in the resonant tunneling frequency, f_1. Therefore, the two parameters of the well half-width, a, and the barrier thickness, b, with the aluminum content, y, can be used to adjust the frequency of the diode device to operate at the desired frequency in the tera range.

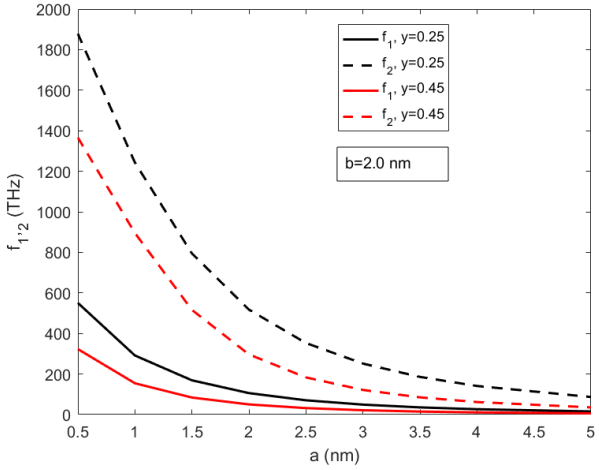

Figure 5: Dependence of both the Resonant Tunneling Frequencies for the Lowest, f_1 (tHz) (Solid Lines), and First Excited States, F_2 (thz) (Dashed Lines), on the Well Half-Width, a, in Nm at a Constant Barrier Thickness, B, Of 2.0 Nm for Two Aluminum Contents, y = 0.25 and 0.45

Figure 5 depicts a comparison of the dependence of both the resonant tunneling frequency related to the lowest state, f_1 (THz), and the first excited state, f_2 (THz), on the well half-width, a, at a constant barrier thickness, b, of 2.0 nm and for two aluminum contents, y. Figure 5 shows the exponential decay trend of both frequencies as the well half-width, a, increases. It is also seen in Figure 5 that the lowest tunneling frequency, f_1 (solid line), is lower than the first excited state, f_2 (dashed line). This finding is due to the fact that the resonant tunneling lifetime of the lowest state is longer than that associated with the first excited state.

Figure 6 demonstrates the variation of the resonant tunneling frequencies related to the lowest state, f_1 (THz), and that associated with the first excited state, f_2 (THz), with the barrier thickness, b, at a constant well half-width, a, of 2.5 nm for different aluminum contents, y. It is seen in Figure 6 that for any aluminum content, y, the lowest and first excited resonant tunneling frequencies decrease exponentially as the barrier thickness, b, increases. It is also shown in Figure 6 that the lowest resonant tunneling frequency, f_1 (solid line), is lower than the frequency associated with the first excited state, f_2 (dashed line).

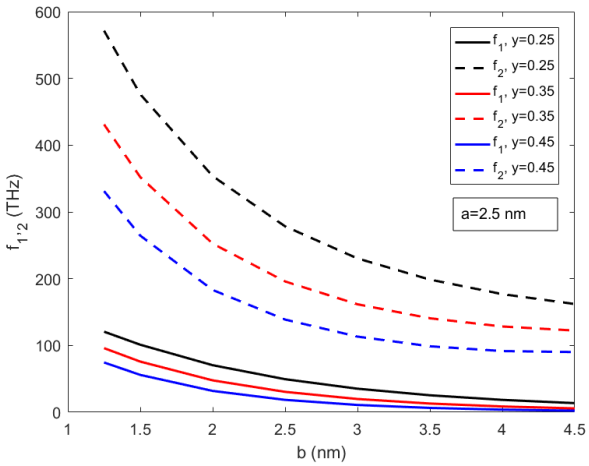

Figure 6: Dependence of the Resonant Frequencies in thz of the Lowest, F_1 (Solid Lines), and First Excited, F_2 (Dashed Lines), Resonant Tunneling on the Barrier Thickness, b, in Nm at Constant Well Half-Width, a, of 2.5 Nm for Different Aluminum Contents, y = 0.25, 0.35, and 0.45

Figure 7 illustrates the relationship between the resonant tunneling current, I_r, for the lowest and first excited states, measured in μA, and the aluminum content, y. Increasing the concentration of aluminum in the $Ga_{1-y}Al_yAs$ barrier layer of the collector enhances the height of the potential barrier, U_0, delays the time for electrons to cross the barrier, and reduces the resonant frequency, resulting in a decrease in resonant energy.

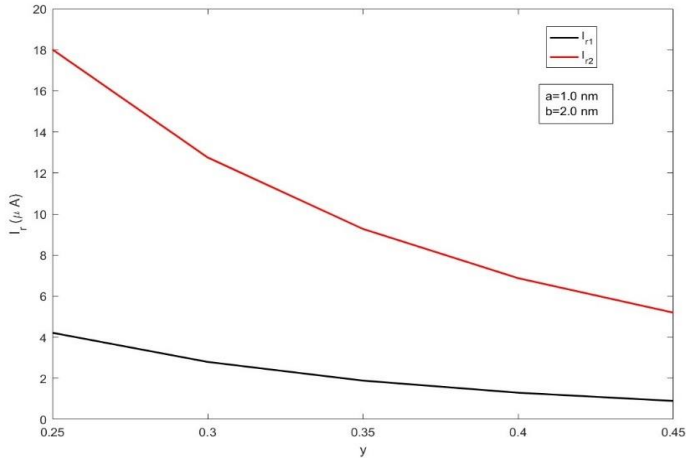

Figure 7: Dependence of both the Resonant Tunneling Currents for the Lowest, I^1 (μA) (Black Line), and the First Excited States, I_2 (μA) (Red Line), on the Aluminum Content, y at a Constant Well Half-Width, a=1.0 nm, and a Barrier Thickness, b=2.0 nm

Figure 8 shows how the resonant tunneling of the lowest state, I_1 (μA), depends on the barrier thickness, b. This is at a constant aluminum content of y=0.25 and a well-half thickness of a=2.5 nm. The results indicate that the resonant tunneling current reduces as the thickness of the collector barrier increases. The increase in barrier thickness in the collector region slows current flow by causing electrons to take longer to cross the barrier. This leads to a reduction in resonant frequency and a decrease in resonance peak current. Similar results are achieved for the resonant tunneling current corresponding to the first excited state. Calculations were also conducted to analyze how the resonant current varies with the well width while keeping the aluminum content and the barrier thickness constants. Enhancing the width of the well was discovered to decrease the resonant peak current. Increasing the width of the well reduces the energy and prolongs the lifetime of electrons, resulting in a lower frequency and decreased resonant tunneling current.

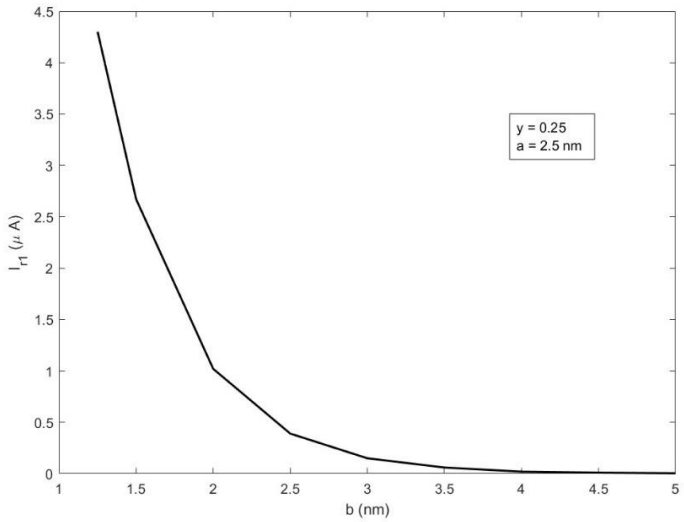

Figure 8: Dependence of the Resonant Tunneling Current for the Lowest State, I_{r1} (μA) on the Collector Barrier Thickness b (nm) at a Constant Aluminum Content, y=0.25 and a Well Half-Width, a=2.5 nm

These findings for the resonant tunneling current for a nanostructured diode with a two-fold symmetrical right triangular barrier are in good agreement with the results of H. Wang et al. [33], who calculated the peak current density for symmetrical triangular double-barrier (TDB) structures which decreases with increasing the collector barrier thickness.

Conclusions

The present investigation explored the impact of physical properties such as size (shape), aluminum content, and effective mass on the resonant frequency, associated resonant energy, and the current peak of a nanostructured diode with a two-fold right triangular barrier composed of GaAs/Ga1-yAlyAs semiconductor materials. The resonant tunneling energy of the lowest and first excited states depends significantly on the well half-width, barrier thickness, electron effective mass, and aluminum concentration. It was noted that reducing the diode's well width and barrier thickness led to an increase in the resonant tunneling frequency for the lowest and first excited states. The resonant tunneling frequency for the first excited state was higher than that for the lowest (ground) state. The effect of the well width on the two resonant frequencies is determined to be more significant than that of the barrier thickness. Additionally, the resonant tunneling frequencies of both the lowest and first excited states increased by reducing the aluminum content in the barrier region of the structure. The resonant tunneling current was calculated and found to be highly influenced by the aluminum content, collector barrier thickness, and well width. It has been observed that the tunneling current peak behavior aligns well with what has been previously outlined in the literature regarding current density peaks. Specifically, the peaks reduce in magnitude as the thickness of the collector barrier increases. Additionally, the structural features of the nanostructured diode with a two-fold right triangular barrier significantly impact the diode's resonant tunneling energy, frequency, and current. These factors can be adjusted to optimize the diode's performance for specific frequency ranges and peak current levels.

• Data availability statement

The data that support the findings of this study are openly available at demand.

• Conflicts of interest

The authors declare no competing interests.

• Funding

This research did not receive any specific grant from funding agencies in the public, commercial, or not-for-profit sectors.

References

1. Kitai, A. (2011). Principles of Solar Cells, LEDs and Diodes: The role of the PN junction. John Wiley & Sons.
2. Ling, J. (1999). Resonant tunneling diodes: Theory of operation and applications. University of Rochester, Rochester, NY, 14627.
3. Molina-Reyes, J., Uribe-Vargas, H., Ortega, E., & Ponce, A. (2018). Resonant tunneling MIIIS diode based on intrinsic quantum-well formation of ultra-thin atomic layered films after band-offset engineering. *Applied Surface Science, 458*, 166-171.
4. Capasso, F., Mohammed, K., & Cho, A. (1986). Resonant tunneling through double barriers, perpendicular quantum transport phenomena in superlattices, and their device applications. *IEEE Journal of Quantum Electronics, 22*(9), 1853-1869.
5. L. Esaki and R. Tsu, Superlattice and negative differential conductivity in semiconductors. IBM J. Res. Dev. 14 (1970) 61-65; Tsu R. and Esaki L. Tunneling in a finite superlattice. *Appl. Phys. Lett. 22* (1973) 562-564.
6. Wasa, K. (2012). Handbook of sputter deposition technology: fundamentals and applications for functional thin films, nano-materials and MEMS. William Andrew.

7. Ludowise, M. J. (1985). Metalorganic chemical vapor deposition of III-V semiconductors. *Journal of Applied Physics, 58*(8), R31-R55.
8. Mendez, E. E., Wang, W., Ricco, B., & Esaki, L. (1985). Resonant tunneling of holes in AlAs-GaAs-AlAs heterostructures. *Applied physics letters, 47*(4), 415-417.
9. Mendez, E. E., Esaki, L., & Wang, W. I. (1986). Resonant magnetotunneling in GaAlAs-GaAs-GaAlAs heterostructures. *Physical Review B, 33*(4), 2893.
10. Mendez, E. E., Calleja, E., Da Silva, C. G., Chang, L. L., & Wang, W. I. (1986). Observation by resonant tunneling of high-energy states in GaAs-Ga 1− x Al x as quantum wells. *Physical Review B, 33*(10), 7368.
11. Lunz, U., Keim, M., Reuscher, G., Fischer, F., Schüll, K., Waag, A., & Landwehr, G. (1996). Resonant electron tunneling in ZnSe/BeTe double-barrier, single-quantum-well heterostructures. *Journal of applied physics, 80*(11), 6329-6332.
12. Liu, H. C. (1987). Resonant tunneling through single layer heterostructures. *Applied physics letters, 51*(13), 1019-1021.
13. Alexander, M. G. W., Nido, M., Rühle, W. W., & Köhler, K. (1990). Resonant-tunneling transfer times between asymmetric GaAs/Al 0.35 Ga 0.65 As double quantum wells. *Physical Review B, 41*(17), 12295.
14. Guo, D. F., Laih, L. W., Tsai, J. H., Liu, W. C., & Hsu, W. C. (1995). Characteristics of a GaAs-InGaAs quantum-well resonant-tunneling switch. *Journal of applied physics, 77*(6), 2782-2785.
15. Mounaix, P., Libberecht, J. M., & Lippens, D. (1995). Electron transfer between two coupled quantum wells in a resonant tunneling diode structure. *Solid-State Electronics, 38*(11), 1899-1904.
16. Allen, S. S., & Richardson, S. L. (1996). Improved Airy function formalism for study of resonant tunneling in multibarrier semiconductor heterostructures. *Journal of applied physics, 79*(2), 886-894.
17. Elabsy, A. M. (2000). Effective mass dependence of resonant quasi-level lifetime in GaAs–AlxGa1− xAs double-barrier structures. *Physica B: Condensed Matter, 292*(3-4), 233-237.
18. Elkenany, E. B., & Elabsy, A. M. (2022). Comparative investigation between complex energy and transfer matrix techniques for quasi-energy states in heterostructure materials. *Journal of Materials Science: Materials in Electronics, 33*(28), 22469-22479.
19. Elkenany, E. B., & Elabsy, A. M. (2022). Impact of pressure on the resonant energy and resonant frequency for two barriers Ga1− xAlxAs/GaAs nanostructures. *Physica Scripta, 98*(1), 015809.
20. Romeira, B., Pessoa, L. M., Salgado, H. M., Ironside, C. N., & Figueiredo, J. M. (2013). Photo-detectors integrated with resonant tunneling diodes. *Sensors, 13*(7), 9464-9482.
21. A. Pfenning, et al. Sensitivity of resonant tunneling diode photodetectors. Nanotechnology 27 (2016) 355202.
22. Davidovich, M. V. (2019). Time-dependent resonant tunneling in a double-barrier diode structure. *Jetp Letters, 110*, 472-480.
23. Yadav, S. L., & Najeeb-Ud-Din, H. (2020). A simple analytical model for the resonant tunneling diode based on the transmission peak and scattering effect. *Journal of Computational Electronics, 19,* 1061-1067.
24. Elabsy, A. M., & Elkenany, E. B. (2022). Effect of the nonparabolicity on the resonant lifetimes and resonant energies of symmetric GaAs/AlxGa1-xAs double barrier nanostructures. *Physica B: Condensed Matter, 632*, 413711.
25. Meem, T. A., Torsa, S. T., Hasan, M., & Rahman, M. (2023). A Comparative Study of Fixing One Barrier Varying Another Barrier for a Resonant Tunneling Diode.
26. Tkach, N. V., & Golovatskii, V. A. (2001). Quasi-stationary states of electrons and holes in an open composite cylindrical quantum wire. *Physics of the Solid State, 43*, 365-372.
27. Krive, I. V., Palevski, A., Shekhter, R. I., & Jonson, M. (2010). Resonant tunneling of electrons in quantum wires. *Low Temperature Physics, 36*(2), 119-141.
28. Tkach, N. V., & Golovatskii, V. A. (1999). Quasistationary states of an electron in a spherical β-HgS/β-CdS/β-HgS nanoheterosystem. *Physics of the Solid State, 41,* 1911-1913.
29. Su, X., Chakrabarti, S., Bhattacharya, P., Ariyawansa, G., & Perera, A. U. (2005). A resonant tunneling quantum-dot infrared photodetector. *IEEE journal of quantum electronics, 41*(7), 974-979.
30. Biswas, S. K., Schowalter, L. J., Jung, Y. J., Vijayaraghavan, A., Ajayan, P. M., & Vajtai, R. (2005). Room-temperature resonant tunneling of electrons in carbon nanotube junction quantum wells. *Applied Physics Letters, 86*(18).
31. Davidovich, M. V., Nefedov, I. S., Glukhova, O. E., & Slepchenkov, M. M. (2021). Toward the theory of resonant-tunneling triode and tetrode with CNT–graphene grids. *Journal of Applied Physics, 130*(20).
32. Ohmukai, M. (2005). Triangular double barrier resonant tunneling. *Materials Science and Engineering: B, 116*(1), 87-90.
33. Wang, H., Xu, H., & Zhang, Y. (2006). A theoretical study of resonant tunneling characteristics in triangular double-barrier diodes. *Physics Letters A, 355*(6), 481-488.
34. Chandrasekar, L. B., Karunakaran, M., & Muthukumar, P. (2023). A study of tunneling in triangular resonant tunnel diodes: Effect of barrier width, barrier height, pressure, temperature, and heterostructure strain. *Micro and Nanostructures, 178*, 207564.
35. Elabsy, A. M., & Attia, M. T. (2023). Quasi-resonant tunneling states in triangular double-barrier nanostructures. *J Math Techniques Comput Math, 2*(8), 347-355.
36. Elabsy, A. M., & Attia, M. T. (2023). Resonant tunneling of electrons in biased symmetric triangular double barrier nanostructure triodes. *Physica Scripta, 98*(10), 105920.
37. Kumar Mishra, S., Kumar, A., Prakash Kaushik, C., & Dikshit, B. (2017). Resonant tunneling effect in graphene superlattice heterostructures by tuning the electric potential of defect layer. *Journal of Applied Physics,*

121(18).
38. Choi, W., Choudhary, N., Han, G. H., Park, J., Akinwande, D., & Lee, Y. H. (2017). Recent development of two-dimensional transition metal dichalcogenides and their applications. *Materials Today, 20*(3), 116-130.
39. Wang, J., Al-Khalidi, A., Alharbi, K., Ofiare, A., Zhou, H., Wasige, E., & Figueiredo, J. (2016, October). High performance resonant tunneling diode oscillators as terahertz sources. In *2016 46th European Microwave Conference (EuMC)* (pp. 341-344). IEEE.
40. Miyamoto, T., Yamaguchi, A., & Mukai, T. (2016). Terahertz imaging system with resonant tunneling diodes. *Japanese Journal of Applied Physics, 55*(3), 032201.
41. Asada, M., & Suzuki, S. (2021). Terahertz emitter using resonant-tunneling diode and applications. *Sensors, 21*(4), 1384.
42. BenDaniel, D. J., & Duke, C. B. (1966). Space-charge effects on electron tunneling. *Physical review, 152*(2), 683.
43. Adachi, S. (1985). GaAs, AlAs, and Al x Ga1− x as: Material parameters for use in research and device applications. *Journal of applied physics, 58*(3), R1-R29.
44. Lee, H. J., Juravel, L. Y., Woolley, J. C., & Thorpe, A. S. (1980). Electron transport and band structure of Ga 1− x Al x as alloys. *Physical Review B, 21*(2), 659.
45. Kopf, R. F., Herman, M. H., Schnoes, M. L., Perley, A. P., Livescu, G., & Ohring, M. (1992). Band offset determination in analog graded parabolic and triangular quantum wells of GaAs/AlGaAs and GaInAs/AlInAs. *Journal of applied physics, 71*(10), 5004-5011.
46. Li, H. W., & Wang, T. H. (2001). Resonant tunneling through energy states of InAs quantum dots in GaAs metal–semiconductor diode structures. *Physica B: Condensed Matter, 304*(1-4), 107-111.
47. M. A. Morrison, Understanding quantum physics. Prentice-Hall, Inc. N. J. (1990) ch.8.